JACS
JOURNAL OF THE AMERICAN CHEMICAL SOCIETY

Communication

pubs.acs.org/JACS

Hole-Transporting Materials with a Two-Dimensionally Expanded π-System around an Azulene Core for Efficient Perovskite Solar Cells

Hidetaka Nishimura,[†] Naoki Ishida,[‡] Ai Shimazaki,[†] Atsushi Wakamiya,*[,†,§] Akinori Saeki,*[,‡] Lawrence T. Scott,*[,∥] and Yasujiro Murata*[,†]

[†]Institute for Chemical Research, Kyoto University, Uji, Kyoto 611-0011, Japan

[‡]Department of Applied Chemistry, Graduate School of Engineering, Osaka University, 2-1 Yamadaoka, Suita, Osaka 565-0871, Japan

[§]Precursory Research for Embryonic Science and Technology (PRESTO), Japan Science and Technology Agency, 4-1-8 Honcho, Kawaguchi, Saitama 332-0012, Japan

[∥]Merkert Chemistry Center, Boston College, Chestnut Hill, Massachusetts 02467-3860, United States

Supporting Information

ABSTRACT: Two-dimensionally expanded π-systems, consisting of partially oxygen-bridged triarylamine skeletons that are connected to an azulene (**1**−**3**) or biphenyl core (**4**), were synthesized and characterized. When tetrasubstituted azulene **1** was used as a hole-transporting material (HTM) in perovskite solar cells, the observed performance (power conversion efficiency = 16.5%) was found to be superior to that of the current HTM standard Spiro-OMeTAD. A comparison of the hole mobility, the ability to control the HOMO and LUMO levels, and the hole-collection efficiency at the perovskite/HTM interface in **1** with reference compounds (**2**−**4** and Spiro-OMeTAD) led to the elucidation of key factors required for HTMs to act efficiently in perovskite solar cells.

Perovskite solar cells represent attractive cost-effective next generation printable photovoltaics.[1] In this type of solar cells, perovskite semiconductors, such as lead halide perovskite $CH_3NH_3PbI_3$, act as photoabsorbers to generate free carriers that can be collected in the electrodes through both p- and n-type buffer layers.[2] In a relatively short period, power conversion efficiencies (PCEs) in such cells have been substantially increased, mainly due to improvements of the fabrication protocols for the perovskite layer.[3] Although tremendous efforts have been devoted to the development of improved hole-transporting materials (HTMs) for buffer layers,[4,5] the number of high-performance HTMs is still limited.[5] Therefore, 2,2′,7,7′-tetrakis-(*N*,*N*-di-*p*-methoxyphenylamine)-9,9′-spirobifluorene (Spiro-OMeTAD), which is traditionally used for solid-state dye-sensitized solar cells,[6] remains, despite its high cost, the standard buffer material even in perovskite solar cells. For further improvements of the PCE, the development of more cost-effective next-generation HTMs based on new molecular design concepts, and the elucidation of the key factors that determine the photovoltaic performance in perovskite solar cells, will be crucial.

Conventional HTMs for perovskite solar cells are often based on triarylamine skeletons with propeller-like structures.[4,5] We have recently reported that the use of partially oxygen-bridged triarylamines as quasiplanar scaffolds for charge-transporting materials facilitates delocalized π-conjugation and on-top π-stacking in the solid state, which ensures high carrier mobilities in the π-stacking direction.[7] In this study, we designed and synthesized the two-dimensionally expanded system **1** with a sheet-shaped structure, in which four oxygen-bridged triarylamines that contain alkoxy groups to enhance the solubility were attached to a core skeleton (Figure 1). For the core skeleton, we

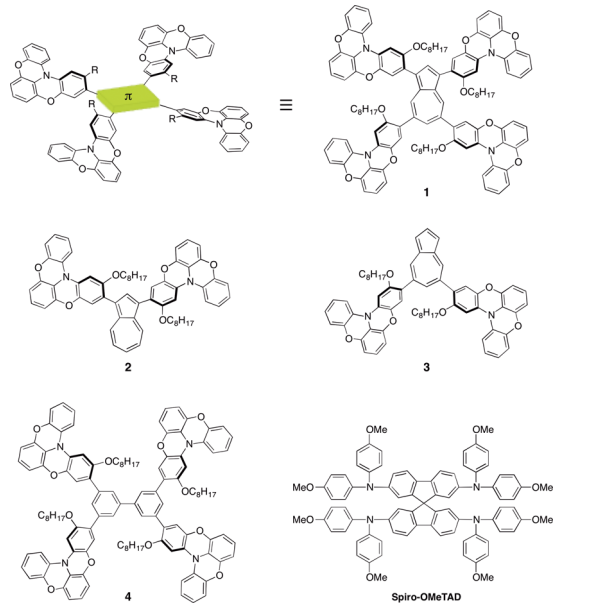

Figure 1. Molecular design for the HTMs in this study together with structures of **1**−**4** and Spiro-OMeTAD.

selected azulene, which is a nonbenzenoid aromatic hydrocarbon[8] that exhibits unique electron-donating and accepting character arising from the five- and seven-membered ring, respectively. Using **1** as a HTM in perovskite solar cells led to high PCEs (16.5%), even when compared to Spiro-OMeTAD. By comparison with reference compounds **2** (1,3-disubstituted azulene), **3** (5,7-disubstituted azulene), **4** (3,3′,5,5′-tetra-substituted 1,1′-biphenyl), and Spiro-OMeTAD, we were able

Received: October 27, 2015
Published: December 10, 2015

DOI: 10.1021/jacs.5b11008
J. Am. Chem. Soc. 2015, 137, 15656−15659

to determine the key factors that improve the efficiency of HTMs in perovskite solar cells, which ultimately led to an increase in cell performance.

The oxygen-bridged triarylamine used in this study was prepared according to a previously reported synthetic method (Scheme S1).[7] Treatment of this triarylamine with 1 equiv of NBS led to a selective monobromination at the octyloxy-substituted ring. 1,3,5,7-Tetra(Bpin)azulene and 3,3′,5,5′-tetra(Bpin)-1,1′-biphenyl were obtained from exhaustive Ir-catalyzed direct borylation of azulene and biphenyl, respectively.[9] 5,7-Di(Bpin)-azulene could be obtained from the selective deborylation of 1,3,5,7-tetra(Bpin)azulene.[9b] These readily available borylated azulene derivatives enable a facile synthesis of the target compounds by conventional Suzuki−Miyaura cross-coupling reactions. Thus, tetra-substituted azulene **1** was generated from the reaction of the monobrominated oxygen-bridged triarylamine and 1,3,5,7-tetra(Bpin)azulene. Reference compounds **2**−**4** were obtained in a similar manner from the corresponding brominated and borylated derivatives (for details, see SI). Compounds **1**−**4** were characterized by NMR, HRMS, and elemental analysis. All new compounds exhibited good solubility in common organic solvents (e.g., >100 mg/mL in chlorobenzene) and high thermal stability (e.g., T_{d5} > 400 °C).

DFT calculations at the B3LYP/6-31G(d) level of theory showed that the Kohn−Sham (KS)-HOMOs of 1,3,5,7-tetra-substituted **1** (−4.23 eV) and 1,3-disubstituted **2** (−4.42 eV) are delocalized over the entire π-conjugated skeleton, including the azulene core (Table 1, Figure S5). The calculated KS-HOMO levels reflect the high electron-donating ability of the five-membered azulene ring. In comparison to **1** and **2**, the KS-HOMO levels in 5,7-disubstituted **3** (−4.60 eV) and **4** with a biphenyl core (−4.61 eV) are lower. The KS-LUMOs of **1**−**3** are localized on the azulene core.

Table 1. Electrochemical and Photophysical Data for 1−4

compd	$E_{1/2,\ ox}$[a] [V]	λ_{sol}[b] [nm] (log ε)	KS-HOMO[c] [eV]	HOMO[d] [eV]
1	+0.00, +0.27	705 (2.92)	−4.23	−5.04
	+0.37,[e] +0.63	446 (4.58)		
		392 (4.75)		
2	+0.09, +0.24	613 (2.49)	−4.42	−5.12
	+0.51	386 (4.57)		
3	+0.41[e]	717 (2.67)	−4.60	−5.42
		644 (3.03)		
		392 (4.56)		
4	+0.26[f]	383 (4.81)	−4.61	−5.27
		316 (4.42)		
Spiro-OMeTAD	+0.05, +0.16	385 (4.88)	−4.21	−5.08
	+0.36[e]	307 (4.75)		

[a]Half-wave oxidation potentials (vs Fc/Fc^+) measured by cyclic voltammetry in CH_2Cl_2 (0.5 mM; supporting electrolyte: 0.1 M [(n-Bu)$_4$N][PF_6]). [b]UV−vis absorption in CH_2Cl_2 (10^{-5} M). [c]Kohn−Sham HOMO level calculated at the B3LYP/6-31G(d) level of theory. [d]HOMO levels estimated from the onset potentials of the first oxidation peak in the cyclic voltammograms (HOMO = −(E_{onset} + 5.1 eV)).[10] [e]Corresponding to a two-electron oxidation. [f]Corresponding to a four-electron oxidation.

The electrochemical and photophysical properties of **1**−**4** are summarized in Table 1. The cyclic voltammogram of **1** in CH_2Cl_2 shows four reversible oxidation waves, indicating the stability of the cationic species. As predicted by DFT calculations, the experimentally observed first oxidation potentials (all potentials vs Fc/Fc^+) of **1** and **2** are lower (**1**, +0.00 V; **2**, +0.09 V) than those of **3** (+0.41 V) and **4** (+0.26 V). The HOMO levels estimated from these potentials are included in Table 1. In the UV−vis absorption spectrum, **1**−**4** exhibit an intense absorption in the UV and/or short wavelength visible region (<450 nm), associated with a π−π^* transition. In addition, azulene derivatives **1**−**3** exhibit a very weak and broad peak in the visible region, corresponding to the intramolecular charge transfer transition of the azulene moiety.

In order to investigate the performance of **1**−**4** in perovskite solar cells, we fabricated such devices using **1**−**4** as HTMs. Our standard cells were based on the following structure: FTO/compact-TiO_2 (30 nm)/mesoporous-TiO_2 (200 nm)/perovskite $CH_3NH_3PbI_3$ (250 nm)/HTM (250 nm)/Au (80 nm). The perovskite layers were prepared according to our optimized sequential two-step solution method.[11] The use of purified solvents and materials, such as CH_3NH_3I and PbI_2, has proven to be essential in order to achieve good results (PCE = 13.4 ± 0.5%), both in terms of performance and reproducibility (Figure S9).

Hole-transport layers (HTLs) of 250 nm thickness were deposited under an inert atmosphere (N_2) on the perovskite layer by spin-coating a chlorobenzene solution of the HTM with additives, such as, e.g., a Co(III)-based oxidizing agent (FK209),[12] lithium bis(trifluoromethane)sulfonamide (LiTFSI), and 4-*tert*-butylpyridine. In order to examine the effect of the amount of oxidizing agent on the solar cell performance, we initially screened the amount of Co(III) dopant in **1**. Upon gradually increasing the amount of oxidant from 0.0 equiv (PCE = 4.8%) to 0.20 equiv (PCE = 14.8%), a significant increase in the solar cell performance was observed, exhibiting a maximum for 0.15 equiv (PCE = 15.7%; Figure S10). The observed PCE is significantly higher than that using Spiro-OMeTAD under identical conditions (PCE = 13.6% with 0.10 equiv of Co(III) dopant) and thus demonstrates the superior performance of **1** as a HTM. In the cell using **1** (Figure 2a, Table 2), the observed short-circuit photocurrent density (J_{SC} = 20.7 mA/cm^2) was comparable to that of a cell using Spiro-OMeTAD (J_{SC} = 21.0 mA/cm^2), while the increases in open-circuit voltage (V_{OC} = 1.04 V) and fill factor (FF = 0.73) were remarkably higher relative to the Spiro-OMeTAD cell (V_{OC} = 0.96 V, FF = 0.68). Cells containing reference compounds **2**−**4** were also prepared using the same two-step method for the preparation of the perovskite layer. Even after screening the amount of Co(III) dopant, only moderate PCEs were obtained for cells using **2** (9.7%, 0.15 equiv) or **3** (8.5%, 0.0 equiv), whereas a cell with **4** showed an even lower

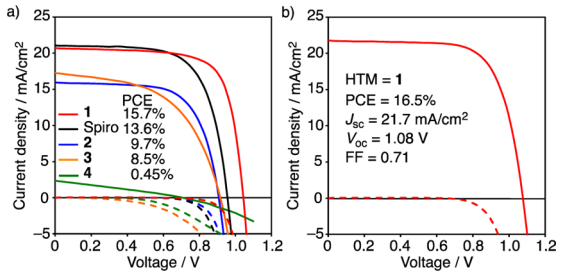

Figure 2. Current density−voltage characteristics for perovskite solar cells with perovskite layers fabricated from (a) a two-step method using **1** (red), **2** (blue), **3** (orange), **4** (green), and Spiro-OMeTAD (black) as HTMs, or from (b) a one-step method using **1** as the HTM; all measurements recorded under a photon flux of 100 mW/cm^2 (AM1.5G, solid line) or in the dark (dashed line).

DOI: 10.1021/jacs.5b11008
J. Am. Chem. Soc. 2015, 137, 15656−15659

Table 2. Summary of Photovoltaic Parameters Derived from *J*–*V* Measurements of Perovskite Solar Cells

HTM	J_{SC} [mA/cm^2]	V_{OC} [V]	FF	PCE [%]	R_s [Ω cm^2]	R_{sh} [Ω cm^2]
1	20.7	1.04	0.73	15.7	8.6	1.6×10^3
1[a]	21.7	1.08	0.71	16.5	6.9	1.9×10^3
2	15.9	0.91	0.67	9.7	4.7	8.2×10^2
3	17.3	0.91	0.54	8.5	8.5	2.7×10^2
4	2.31	0.70	0.28	0.45	180	3.4×10^2
Spiro-OMeTAD	21.0	0.96	0.68	13.6	4.6	2.6×10^3

[a]Fabricated using a one-step method (toluene dropping).

performance (0.45%, 0.15 equiv). Recently, modified one-step solution methods using solvent engineering have been reported as effective methods to prepare flat and dense perovskite layers that provide high PCEs.[3] When cells with **1** were prepared in such a one-step manner (toluene dropping), the PCEs further increased to 16.5% (Figure 2b). This result is even more remarkable, considering that this method has not yet been optimized in our laboratory, which clearly demonstrates the high potential of **1** as a HTM in perovskite solar cells.

To elucidate the factors that enable compounds to act as efficient HTMs in perovskite solar cells, **1**–**4** as well as Spiro-OMeTAD were compared with respect to (1) hole mobility, (2) electronic structure, i.e., HOMO and LUMO levels in bulk films, and (3) charge collection at the HTM/perovskite layer interface. Initially, the hole mobility in neat bulk films of **1**–**4** and Spiro-OMeTAD with a thickness of 200–400 nm, which is comparable to films used in current perovskite solar cells (Figure S14–19), was examined by the space-charge-limited current (SCLC) method (Figure S20). The mobility of **1** (2.1×10^{-4} cm^2/(V s)) was comparable to that of Spiro-OMeTAD (2.7×10^{-4} cm^2/(V s)),[13] and both values were higher than those of **2** (7.6×10^{-5} cm^2/(V s)), **3** (6.3×10^{-6} cm^2/(V s)), and **4** (2.4×10^{-5} cm^2/(V s)). The observed correlation between the hole mobility and the PCE of **1**–**3** and Spiro-OMeTAD indicates a critical importance of a high carrier mobility, which should contribute in particular to high FF values. In order to reveal the local carrier mobility, we also performed time-resolved microwave conductivity (TRMC) measurements.[14] A spin-coated film of **1** exhibited a local mobility ($\Sigma\mu$ = 1.8 cm^2/(V s)), which was four times higher than that of Spiro-OMeTAD ($\Sigma\mu$ = 0.45 cm^2/(V s)), measured under the same conditions (Figure S29). As the HTMs were used in our optimized cells together with oxidizing agents, TRMC measurements were also conducted on Co(III)-doped films of **1**. The TRMC signal ($\phi\Sigma\mu$), corresponding to the product of photogeneration efficiency of the charge carrier (ϕ) and $\Sigma\mu$, increased up to 4–5 times upon addition of 0.05–0.20 equiv of the oxidant (Figure S30). Under the assumption that ϕ remained unchanged in the doped films, this result indicates that Co(III) doping induced a significant increase of the local mobility, which contributes to a reduced series resistance and facilitated ohmic contact with the metal.[15]

Subsequently, we evaluated the HOMO and LUMO levels in bulk films, taking the effects of the oxidizing agents into account. Figure 3 shows the ionization potentials (IPs, HOMO levels) obtained from photoelectron spectroscopy measurements in air for spin-coated films of **1**–**4** and Spiro-OMeTAD containing the previously determined optimum amount of Co(III) dopant. Compared to neat films without oxidant (Figure S28), the IPs of the doped films were decreased by ∼0.1 eV due to partial

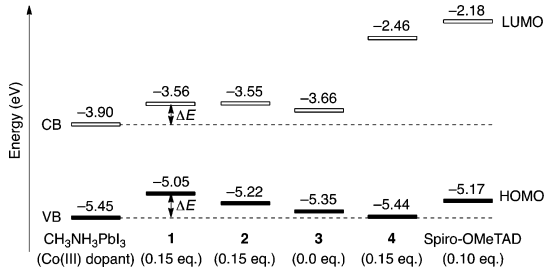

Figure 3. HOMO and LUMO levels of **1**–**4** and Spiro-OMeTAD in doped spin-coated films, determined by photoelectron spectroscopy and optical band gap analysis; the valence and conduction bands of $CH_3NH_3PbI_3$ are included as reference levels.

oxidation. The IPs in **1**–**3** and Spiro-OMeTAD (−5.05 to −5.35 eV, ΔE = +0.10 to +0.40 eV) were higher than that of the valence band (VB) in $CH_3NH_3PbI_3$ (−5.45 eV). In contrast, the IP in **4** (−5.44 eV) was comparable to that of the VB, which means that an effective hole injection from the perovskite to **4** was not possible, consistent with the very low PCE observed. Furthermore, the LUMO levels of **1**–**4** were determined (Figure 3) based on these HOMO levels (IPs), and the optical band gap energies determined from the absorption spectra of the spin-coated films (Figure S8). The LUMO level of **3** (−3.66 eV, ΔE = +0.24 eV) was close to the conduction band (CB) of $CH_3NH_3PbI_3$ (−3.90 eV),[1c] which probably reflects an inefficient electron blocking ability of **3**, thus leading to a relatively small R_{sh}. These results clearly indicate the importance of being able to control the HOMO and LUMO levels of the HTM relative to the VB and CB levels of the perovskite material.

The question why tetra-substituted azulene derivative **1** exhibited a better performance than Spiro-OMeTAD and 1,3-disubstituted azulene **2** still remains to be addressed. For that purpose, we examined the charge collection ability of these HTMs at their interface with the perovskite layer by measuring the transient decay of the TRMC. Recent TRMC studies on perovskite materials revealed a TRMC signal ($\phi\Sigma\mu$) for perovskite on a mesoporous TiO_2 layer that was by 2 orders of magnitude higher than those of organic HTMs such as Spiro-OMeTAD.[14b] Accordingly, the charge collection ability of HTMs from the perovskite layer can be evaluated by the intensity decrease of the TRMC transient after deposition of the HTM onto the perovskite layer. Figure 4 shows the transient TRMC decay prior and posterior to HTM coating. Only a moderate decrease of peak intensity ($\Delta\phi\Sigma\mu$) and delay time was observed for **2**, whereas a significant decline was observed for both **1** and Spiro-OMeTAD. This result indicates that the latter HTM coatings effectively quench the perovskite conductivity, showing

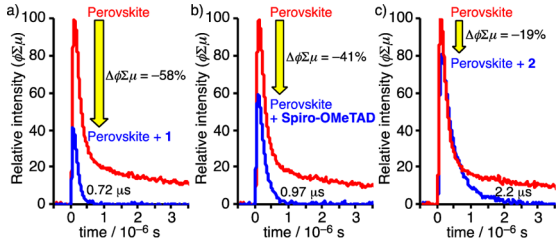

Figure 4. TRMC transients (normalized $\phi\Sigma\mu$) of perovskite films prior (red) and posterior (blue) to HTM coating at a photon flux of $I_0 = 1.4 \times 10^{11}$ photons/cm^2. HTM/dopant: (a) **1**/0.15 equiv of Co(III), (b) Spiro-OMeTAD/0.10 equiv of Co(III), and (c) **2**/0.15 equiv of Co(III).

DOI: 10.1021/jacs.5b11008
J. Am. Chem. Soc. 2015, 137, 15656–15659

efficient hole-collection ability of the HTM to yield high J_{SC}, V_{OC}, and FF values. In the profile for **1**, the magnitude of peak suppression was higher ($\Delta\phi\Sigma\mu = -58\%$) and the speed of decay faster ($t = 0.72\ \mu s$) than that of Spiro-OMeTAD ($\Delta\phi\Sigma\mu = -41\%$, $t = 0.97\ \mu s$) or **2** ($\Delta\phi\Sigma\mu = -19\%$, $t = 2.2\ \mu s$). These results suggest that the horizontal, face-on molecular orientation of the HTMs on the perovskite layer, which could facilitate charge collection, is most likely enhanced by the two-dimensionally expanded molecular shape of the π-conjugated skeleton in tetra-substituted azulene **1** relative to disubstituted azulene **2**, which contains a smaller π-system, and Spiro-OMeTAD, which exhibits a spherical shape. It should also be noted that a good correlation was observed between the PCE values of the solar cells and the extent of transient decay in the TRMC measurements (Figures S32 and 33, Table S5). Our results thus demonstrate the utility of this method for the evaluation of device performance and optimal doping conditions for newly synthesized semiconductors prior to the laborious fabrication of solar cells.

In summary, we have described the synthesis of **1**, in which the conjugated π-system is two-dimensionally expanded over four quasiplanar skeletons and a central azulene core. Perovskite solar cells that use **1** as a HTM exhibited a superior performance (PCE $\leq$ 16.5%) relative to those using the current standard Spiro-OMeTAD. Based on the evaluation and a comparison of the optoelectronic and electrochemical properties of **1**−**4** and Spiro-OMeTAD, we were able to elucidate the factors that are required for HTMs to act efficiently in perovskite solar cells: (1) a good hole mobility that can be partly modified by chemical doping; (2) control over the HTM HOMO and LUMO levels, which should be at least 0.1 and 0.25 eV higher than the perovskite VB and CB, respectively; and (3) high hole-collecting ability at the HTM/perovskite interface. With respect to (3), the preferred horizontal molecular orientation of two-dimensionally expanded π-systems should be particularly beneficial. In line with these new molecular design principles, we believe that several more sophisticated HTMs for perovskite solar cells should be easily attainable. Development and optimization of more extended HTMs are currently in progress in our laboratory, and results will be reported in due course.

■ ASSOCIATED CONTENT

Supporting Information

The Supporting Information is available free of charge on the ACS Publications website at DOI: 10.1021/jacs.5b11008.

Experimental details and characterization data (PDF)

■ AUTHOR INFORMATION

Corresponding Authors

*wakamiya@scl.kyoto-u.ac.jp
*saeki@chem.eng.osaka-u.ac.jp
*lawrence.scott@bc.edu
*yasujiro@scl.kyoto-u.ac.jp

Notes

The authors declare no competing financial interest.

■ ACKNOWLEDGMENTS

This study was partially supported by the PRESTO, COI, and ERATO programs from the Japanese Science and Technology Agency (JST) and by the US National Science Foundation and Department of Energy. The authors would like to thank Prof. K. Itami (Nagoya University) for fruitful discussions, and Prof. K. Matsuda and Mr. F. Wang (Kyoto University) for advice on the measurement of SEM images.

■ REFERENCES

(1) For reviews, see: (a) Gao, P.; Grätzel, M.; Nazeeruddin, M. K. *Energy Environ. Sci.* **2014**, *7*, 2448. (b) Miyasaka, T. *Chem. Lett.* **2015**, *44*, 720. (c) Jung, H. S.; Park, N.-G. *Small* **2015**, *11*, 10. (d) Luo, S.; Daoud, W. A. *J. Mater. Chem. A* **2015**, *3*, 8992.

(2) (a) Yamada, Y.; Nakamura, T.; Endo, M.; Wakamiya, A.; Kanemitsu, Y. *J. Am. Chem. Soc.* **2014**, *136*, 11610. (b) Manser, J. S.; Kamat, P. J. *Nat. Photonics* **2014**, *8*, 737. (c) La-o-vorakiat, C.; Salim, T.; Kadro, J.; Khuc, M.-T.; Haselsberger, R.; Cheng, L.; Xia, H.; Gurzadyan, G. G.; Su, H.; Lam, Y. M.; Marcus, R. A.; Michel-Beyerle, M.-E.; Chia, E. E. M. *Nat. Commun.* **2015**, *6*, 7903.

(3) For examples, see: (a) Jeon, N. J.; Noh, J. H.; Kim, Y. C.; Yang, W. S.; Ryu, S.; Seok, S. I. *Nat. Mater.* **2014**, *6*, 897. (b) Xiao, M.; Huang, F.; Huang, W.; Dkhissi, Y.; Zhu, Y.; Etheridge, J.; Gray-Weale, A.; Bach, U.; Cheng, Y.-B.; Spiccia, L. *Angew. Chem., Int. Ed.* **2014**, *53*, 9898. (c) Yang, W. S.; Noh, J. H.; Jeon, N. J.; Kim, Y. C.; Ryu, S.; Seo, J.; Seok, S. I. *Science* **2015**, *348*, 1234. (d) Ahn, N.; Son, D.-Y.; Jang, I.-H.; Kang, S. M.; Choi, M.; Park, N.-G. *J. Am. Chem. Soc.* **2015**, *137*, 8696.

(4) Yu, Z.; Sun, L. *Adv. Energy Mater.* **2015**, *5*, 1500213.

(5) (a) Heo, J. H.; Im, S. H.; Noh, J. H.; Mandal, T. N.; Lim, C.-S.; Chang, J. A.; Lee, Y. H.; Kim, H.; Sarkar, A.; Nazeeruddin, M. K.; Grätzel, M.; Seok, S. I. *Nat. Photonics* **2013**, *7*, 486. (b) Jeon, N. J.; Lee, H. G.; Kim, Y. C.; Seo, J.; Noh, J. H.; Lee, J.; Seok, S. I. *J. Am. Chem. Soc.* **2014**, *136*, 7837. (c) Li, H.; Fu, K.; Hagfeldt, A.; Grätzel, M.; Mhaisalkar, S. G.; Grimsdale, A. C. *Angew. Chem., Int. Ed.* **2014**, *53*, 4085. (d) Li, H.; Fu, K.; Boix, P. P.; Wong, L. H.; Hagfeldt, A.; Grätzel, M.; Mhaisalkar, S. G.; Grimsdale, A. C. *ChemSusChem* **2014**, *7*, 3420. (e) Qin, P.; Paek, S.; Dar, M. I.; Pellet, N.; Ko, J.; Grätzel, M.; Nazeeruddin, M. K. *J. Am. Chem. Soc.* **2014**, *136*, 8516. (f) Gratia, P.; Magomedov, A.; Malinauskas, T.; Daskeviciene, M.; Abate, A.; Ahmad, S.; Grätzel, M.; Getautis, V.; Nazeeruddin, M. K. *Angew. Chem., Int. Ed.* **2015**, *54*, 11409.

(6) Bach, U.; Lupo, D.; Comte, P.; Moser, J. E.; Weissörtel, F.; Salbeck, J.; Spreitzer, H.; Grätzel, M. *Nature* **1998**, *395*, 583.

(7) Wakamiya, A.; Nishimura, H.; Fukushima, T.; Suzuki, F.; Saeki, A.; Seki, S.; Osaka, I.; Sasamori, T.; Murata, M.; Murata, Y.; Kaji, H. *Angew. Chem., Int. Ed.* **2014**, *53*, 5800.

(8) Plattner, P. A.; St. Pfau, A. *Helv. Chim. Acta* **1937**, *20*, 224.

(9) (a) Eliseeva, M. N.; Scott, L. T. *J. Am. Chem. Soc.* **2012**, *134*, 15169. (b) Nishimura, H.; Eliseeva, M. N.; Wakamiya, A.; Scott, L. T. *Synlett* **2015**, *26*, 1578.

(10) Cardona, C. M.; Li, W.; Kaifer, A. E.; Stockdale, D.; Bazan, G. C. *Adv. Mater.* **2011**, *23*, 2367.

(11) Wakamiya, A.; Endo, M.; Sasamori, T.; Tokitoh, N.; Ogomi, Y.; Hayase, S.; Murata, Y. *Chem. Lett.* **2014**, *5*, 711.

(12) Burschka, J.; Kessler, F.; Nazeeruddin, M. K.; Grätzel, M. *Chem. Mater.* **2013**, *25*, 2986.

(13) This value is in good agreement with that obtained from time-of-flight measurement (2×10^{-4} cm^2/V s); see: Poplavskyy, D.; Nelson, J. *J. Appl. Phys.* **2003**, *93*, 341.

(14) (a) Saeki, A.; Koizumi, Y.; Aida, T.; Seki, S. *Acc. Chem. Res.* **2012**, *45*, 1193. (b) Oga, H.; Saeki, A.; Ogomi, Y.; Hayase, S.; Seki, S. *J. Am. Chem. Soc.* **2014**, *136*, 13818.

(15) Shen, Y.; Hosseini, A. R.; Wong, M. H.; Malliaras, G. G. *ChemPhysChem* **2004**, *5*, 16.

DOI: 10.1021/jacs.5b11008
J. Am. Chem. Soc. 2015, 137, 15656−15659